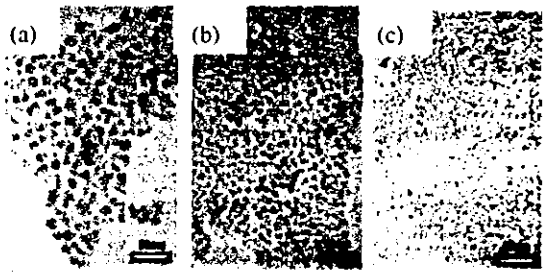

FIG. 3. Size selection by acetone treatment. (a) Product 1, (b) product 3, and (c) product 5.

pendent steric and van der Waals forces support our interpretation and suggest that the size sorting process would have taken place due to reversible coagulation at the secondary minimum.

B. Magnetization measurements

Figure 4(a) shows the zero field cooling (ZFC) and field cooling (FC) magnetization measurements, normalized to the magnetization at room temperature, on the magnetite samples obtained after size selection. The measurements were carried out in the temperature range from 300 to 5K and an applied field of 100 G. The results confirm the effectiveness of our method for nanosize size sorting. A blocking temperature T_b, considered as the temperature at the peak of the ZFC magnetization, which decreases with particle size is observed. The T_b for samples with average particle diameter of 9, 7.2, 5.9, and 4.5 nm were 60, 30, 17, and 7 K, respectively. The observed trend was expected from the anisotropy energy of Fe_3O_4 that is a function of the volume of the particles. In turn, the value of magnetization at ZFC at the lowest temperature, 5 K, was close to zero for the biggest particles that would suggest that most of them are blocked. However, this was not the case for the suspension with the smaller sizes, which indicates that a significant fraction of the particles was still superparamagnetic even at 5 K. This behavior also explains the difference in the coercivity at temperatures below T_b for powders of different average sizes, Fig. 4(b); at 5 K the coercivity was 235, 157, and 56 Oe for 9, 7.2, and 4.5 nm particles, respectively.

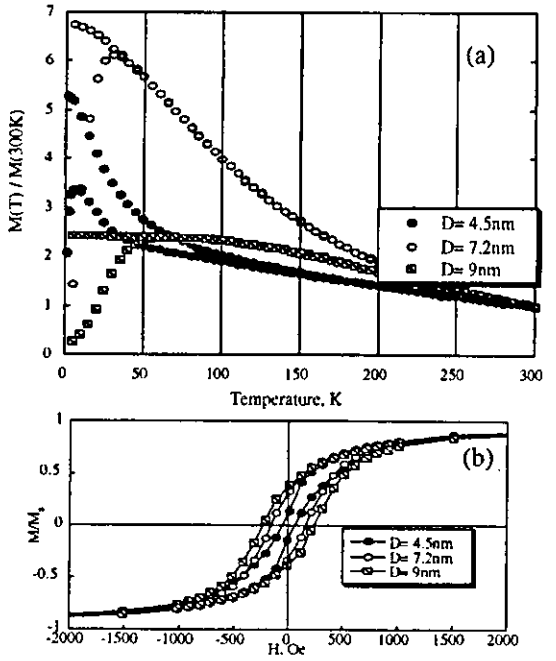

FIG. 4. ZFC and FC measurements (a) and corresponding hysteresis loops at 5 K, (b), for magnetite particles of various diameters, D.

ACKNOWLEDGMENTS

This study was supported by Grant-in-Aid for Basic Research (No. 11565266) and (No. 11450393) from the Ministry of Education, Science, Culture and Sports of Japan and CREST of Japan Science and Technology Institute. The authors thank Kenichi Motomiya for his kind assistance in TEM and HRTEM analyses.

[1]N. Feltin and M. P. Pileni, Langmuir **13**, 3927 (1997).
[2]C. O'Connor and C. Seip, Nanostruct. Mater. **12**, 65 (1999).

Characterization and Structures of Dimeric C_{70} Oxides, $C_{140}O$, Synthesized with Hydrothermal Treatment

Toshiji Kudo, Yuki Akimoto, Kozo Shinoda, Balachandran Jeyadevan, and Kazuyuki Tohji*

Department of Geoscience and Technology, Tohoku University, Sendai, 980-8579, Japan

Takashi Nirasawa

Nihon Bruker Daltonics K.K., Tsukuba, 305-0051, Japan

Markus Waelchli

Bruker Biospin K.K, Tsukuba, 305-0051, Japan

Wolfgang Krätschmer

Max-Planck-Institut für Kernphysik, Postfach 103980, D-69029 Heidelberg, Germany

Received: October 30, 2001; In Final Form: February 4, 2002

The dimeric C_{70} oxides were synthesized from $C_{70}/C_{70}O$ mixed powder by hydrothermal treatment at 373 K for 12 h in aqueous NaOH solution. In this treatment, nucleophilic OH^- ions are abundant and nucleophilic addition reactions were considered to synthesize dimeric fullerene oxides. The yield was estimated as ca. 2−3% summing up each isomer and also produced polyoxides, it is lower than that of $C_{120}O$. Three isomers of $C_{140}O$ were isolated using High Performance Liquid Chromatography (HPLC) and characterized with UV−vis, FT-IR, and ^{13}C NMR and other methods. The results of these methods show a close similarity between $C_{140}O$ and $C_{120}O$ and support that our $C_{140}O$ samples exhibit the structure of conventional furan-bridged dimers. On the basis of the results of ^{13}C NMR and PM3 calculations, structure assignments for each sample were attempted.

1. Introduction

Fullerene oxides are one of the simplest fullerene derivatives and they indicate interesting reaction behavior during synthesis of dimeric species. The synthesis of the dimeric fullerene oxides such as $C_{120}O$ was stimulated by the discovery of the odd-numbered clusters C_{119} in mass spectra of $C_{60}O$[1−3] and Taylor's proposed mechanism for the generation of C_{119} via thermal decarbonylation of $C_{60}O$ and addition of the resultant C_{59} to C_{60}.[4] In fact, $C_{120}O$ has also been synthesized with a mixture of $C_{60}/C_{60}O$[5−7] and Gromov et al. reported the production and characterization of C_{119} synthesized from $C_{120}O$ in large quantities.[8] We also succeeded in the synthesis and isolation of dimeric fullerene oxides such as $C_{120}O$ and three isomers of $C_{130}O$.[9] However, in the earlier reports, the synthesis of $C_{140}O$ using the C_{70} oxides was not accomplished.[10] The reason for this was attributed to weak bonding between C_{70} and the oxygen of $C_{70}O$. Nevertheless, the presence of dimeric C_{70} oxides in the MALDI-TOF mass spectra of $C_{70}O$ suggested the possibility of existence of $C_{140}O$.[11] We believe that $C_{140}O$ could be synthesized in large quantities and may lead to the synthesis of C_{139}. The less symmetrical C_{70} is expected to yield less symmetrical dimers that have complicated structures but have interesting properties. In this work, we report the synthesis of dimeric C_{70} oxides in large quantities using hydrothermal treatment of $C_{70}/C_{70}O$ mixed powder in high pH water.[9,10] In the hydrothermal treatment, nucleophilic OH^- ions are abundant and nucleophilic addition reaction stimulated the synthesis of dimeric fullerene oxides as in C_{120}.[12] At first, OH^- ion attacks $C_{70}O$ and yields intermediate $C_{70}OHO^-$. Then $C_{70}OHO^-$ reacts with neighboring C_{70} to form $(C_{70}OHO-C_{70})^-$. After electron transfers within $(C_{70}OHO-C_{70})^-$, finally $C_{140}O$ is formed releasing OH^- ion. Detailed formation mechanism of dimeric fullerene oxides in hydrothermal treatment is described in ref 9. Hydrothermal treatment can also synthesize water-soluble fullerenes that are believed to be poly-hydroxylated fullerenes, in the case that highly oxidized fullerenes are used as starting material. In this experiment too, water-soluble C_{70} might be synthesized; however, the solution containing the species was removed at the stage of hydrothermal treatment and was not considered for further analysis. Detailed information about the synthesis of water-soluble fullerenes is described elsewhere.[13] Furthermore, we succeeded in isolating three isomers of $C_{140}O$ that were characterized and investigated with several spectroscopic methods.

2. Experiment

2−1. Synthesis and Isolation of Dimeric C_{70} Oxides.

The fullerene C_{70} used in this experiment was extracted and isolated from the fullerene soot synthesized by the arc discharge method using a Soxhlet extractor and HPLC with a Buckyprep column (with a diameter of 20 mm and a length of 250 mm, Nakarai Tesque Co. LTD, Japan) for separation. The purity of the starting material C_{70} was higher than 99%. Then, C_{70} was oxidized by dissolving in toluene and bubbling with ozone. $C_{70}/C_{70}O$ powder was produced by pouring the $C_{70}/C_{70}O$ toluene solution into methanol. Later, dimeric C_{70} oxides were synthe-

* To whom correspondence should be addressed.

10.1021/jp0139989 CCC: $22.00
Published on Web 04/05/2002

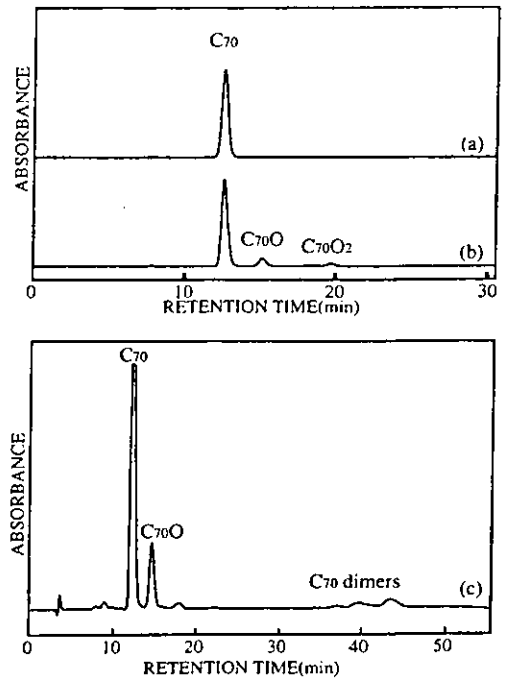

Figure 1. HPLC charts of toluene solution of (a) starting C_{70}, (b) C_{70} after ozone bubbling, and (c) $C_{70}/C_{70}O$ mixture after hydrothermal treatment (Cosmosil Buckyprep column, toluene elution, 330 nm detection).

sized through nucleophilic addition reaction by heating the powder at 373 K for 12 hours in an aqueous NaOH solution of pH 13 or higher. After HPLC analysis with a Buckyprep column (diameter of 4.5 mm and a length of 250 mm) and mass analysis, the product was dissolved in toluene, and a rough separation of dimeric C_{70} oxides from $C_{70}/C_{70}O$ and the isolation of three isomers of $C_{140}O$ were carried out.

2−2. Characterization.

Matrix-Assisted Laser Desorption/Ionization Time-Of-Flight (MALDI-TOF) mass spectra of each sample were measured with a pulsed N_2 laser (337 nm) using 9-nitroanthracene as a matrix (REFLEX III model of Bruker Co. Ltd., Germany). Absorption spectra were measured using a UV−vis spectrophotometer (U-3300 of HITACHI Co. Ltd.). Infrared absorption (IR) spectra were obtained from powder sample embedded in KBr pellets using FT-200 (HORIBA Co.) with resolution of 4 cm^{-1}. Raman spectra were obtained by dropping the sample dissolved in ODCB solutions on brass target and evaporating the solvent. The spectrometer was of type T64000 (Dilor-Jobin Yvon-Spex Co.) with a 514.5-nm wavelength Ar ion laser (Leonix Co.). Finally, ^{13}C NMR spectra were obtained at 125.76 MHz with Cryoprobe DRX500 FT-NMR spectrometer of Bruker. For the measurement, 0.4 mL of saturated solutions (ODCB-d4) of $C_{140}O$ isomers were prepared in a 5-mm NMR tube with ca. 16 mM $Cr(acac)_3$ for paramagnetic relaxation enhancement. Although these samples were not enhanced with ^{13}C, we succeeded in acquiring good spectra with Bruker Cryoprobe. Normal acquisition, resolution enhanced, and spin−echo spectra were used for the identification of the peaks.

3. Results

3−1. Synthesis and Isolation.

Figure 1 a and b show the HPLC charts of C_{70} and $C_{70}/C_{70}O_n$ ($n > 2$) synthesized by ozone bubbling, respectively. New peaks were recorded showing the existence of C_{70} oxides. $C_{140}O$ was

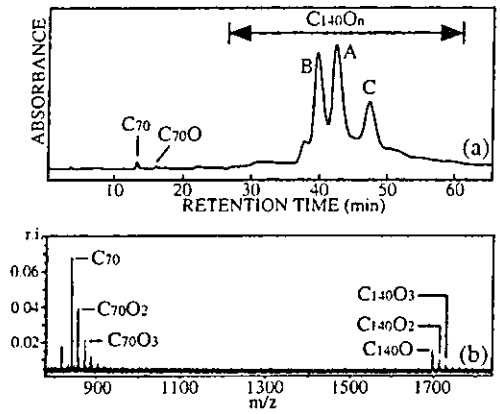

Figure 2. HPLC chart and MALDI-TOF mass spectrum (9-nitroanthracene was used as a matrix) of roughly separated dimeric C_{70} oxides. Relative intensities between monomeric species and dimeric species are different between HPLC chart and mass spectrum. This is caused by fragmentation of $C_{140}O$ in mass spectrometer. HPLC chart shows more reliable data for quantitative analysis.

synthesized using the obtained $C_{70}/C_{70}O_n$ as the starting material. Figure 1c shows the HPLC chart of the substance resulting from hydrothermal treatment. Though the intensities were small, new peaks with long retention time were recorded. The intensities of these new peaks were very low and close to the detectable limit of our HPLC apparatus. Therefore, under the hypothesis that these peaks originate from dimeric C_{70} oxides and their isomers, this region was roughly separated from $C_{70}/C_{70}O_n$ monomer species using HPLC. Then, the sample was evaporated and analyzed using HPLC and MALDI-TOF-MS (Figure 2). $C_{140}O$ has been predicted to have seven isomers by Fowler et al. (Figure 3),[14] and the HPLC analysis showed several peaks suggesting the presence of isomers. On the other hand, not only the presence of $C_{140}O$ but also $C_{140}O_2$ or higher oxides were inferred from the MS analysis of the sample. From these experimental results and the theoretical prediction, this region was believed to include many isomers and polyoxides of $C_{140}O$, for example, $C_{140}O_2$. To examine these polyoxides, we attempted to synthesize $C_{140}O$ from material free of $C_{70}O_2$ prepared using HPLC. Nevertheless, the resulting substance did not show any difference, suggesting nonparticipation of $C_{70}O_2$ in the reaction. We believe that this was due to the low stability of $C_{70}O_2$. With the thermal energy acquired during the experiment, $C_{70}O_2$ could easily dissociate to $C_{70}O$ or C_{70} by releasing oxygen atom. The yield of dimeric C_{70} oxides was estimated as ca. 2−3% summing up the peak area represented by each isomer and polyoxides in the HPLC profile. We believe that the low yield and long retention time prevented the discovery of $C_{140}O$ in the earlier studies.[10]

Figure 4i shows HPLC charts of isolated isomers of $C_{140}O$ marked with A−C in Figure 2. In this figure, HPLC charts of $C_{140}O(A)$ and (B) do not show any difference except for their respective retention times. On the other hand, the peak of C_{70} was recorded only in the chart of $C_{140}O(C)$. To remove this peak, we repeated HPLC separation for $C_{140}O(C)$; however, complete removal of the same was impossible. From the above results, we believe that $C_{140}O(C)$ is an unstable isomer in comparison to A or B. Then, $C_{140}O(C)$ was believed to have dissociated in the process of HPLC separation or during evaporation after HPLC.

Figure 4ii shows MALDI-TOF mass spectra of isolated isomers of $C_{140}O$. Similar to the HPLC result, there was no remarkable difference between mass spectra of $C_{140}O(A)$

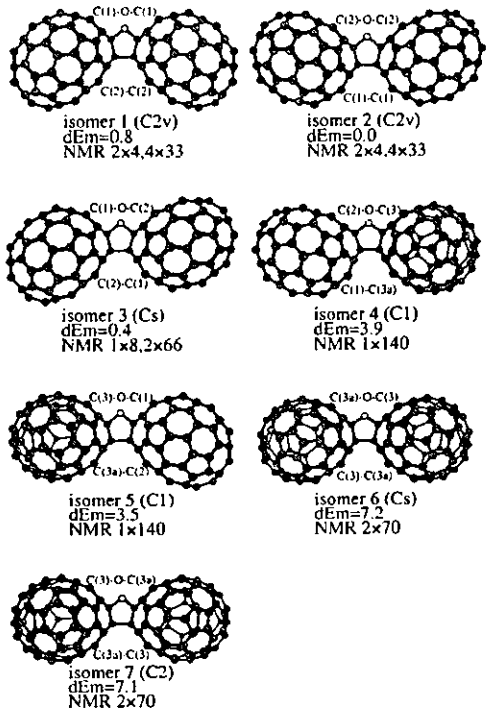

Figure 3. Seven isomers of $C_{140}O$ with their individual symmetry. dEm means relative energy in kJ mol^{-1} calculated with the MNDO model by Fowler et al., and the reliable ^{13}C NMR patterns of intensities are shown. As for the numbering of carbon atoms in C_{70} [C(1)−O−C(1), C(2)−C(2), etc.], refer to Figure 10.

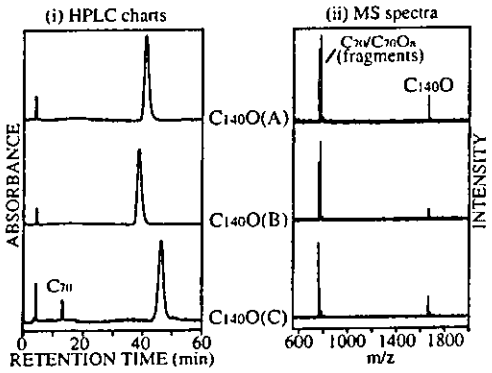

Figure 4. HPLC charts and MALDI-TOF mass spectra of isolated isomers of $C_{140}O$.

and(B); however, mass spectrum of $C_{140}O(C)$ showed less intense mass peak of $C_{70}O$ and more intense mass peaks of poly-oxides of $C_{70}O$ and $C_{140}O$ in comparison to that of $C_{140}O(A)$ and (B). From these results, we conclude that the oxygen atom in $C_{140}O(C)$ easily dissociates and attaches to an adjacent molecule compared to $C_{140}O(A)$ and (B).

3−2. Electronic Absorption.

The UV−vis absorption spectra of each of the isomers of $C_{140}O$ were similar to that of C_{70}, but the bands are broadened and shifted. These differences may result from the less symmetrical structure of $C_{140}O$. The onset seemed to be at slightly longer wavelength compared to C_{70}. In C_{140},[15] the HOMO−LUMO gap has been ascertained both theoretically and experimentally to be smaller than C_{70}. $C_{140}O$ could also be expected to have smaller HOMO−LUMO gap compared to C_{70}. Typical tendencies were also observed in the spectra of other dimeric fullerene oxides such as $C_{120}O$ and $C_{130}O$.

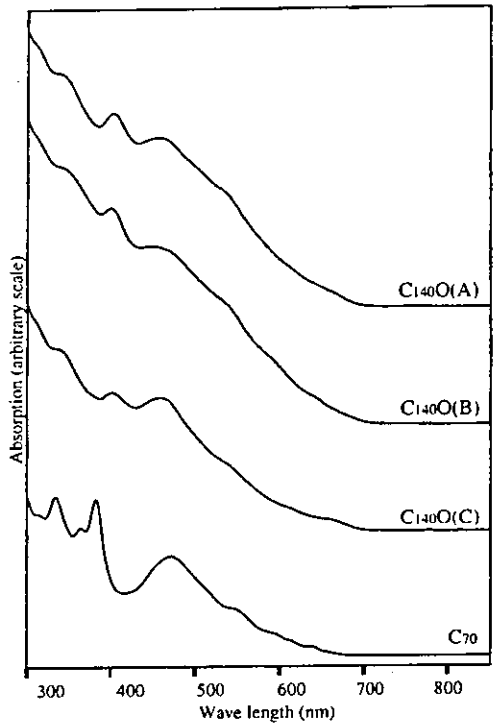

Figure 5. UV−vis absorption spectra of isolated isomers of $C_{140}O$ (upper three spectra) and C_{70} (bottom).

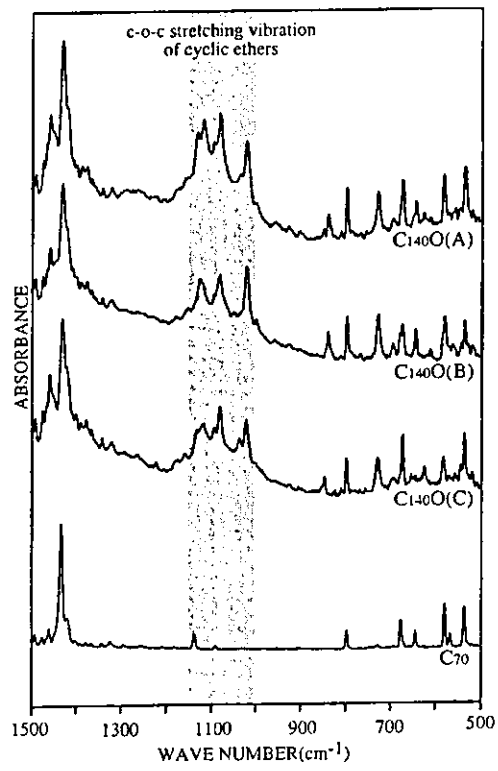

Figure 6. FT-IR absorption spectra of isolated isomers of $C_{140}O$ (upper three spectra) and C_{70} (bottom).

3−3. Vibrational Spectroscopy.

Figure 6 shows FT-IR spectra of isolated isomers of $C_{140}O$. Each isomer showed peaks similar to that of C_{70}; however, they were shifted and split. This is caused by the reduced symmetry

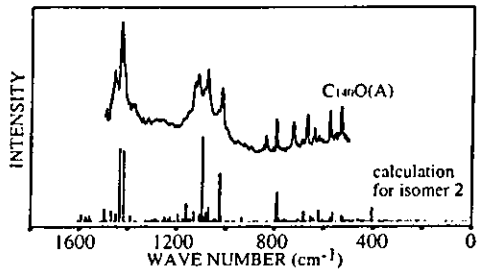

Figure 7. Calculated IR spectrum of $C_{140}O$ isomer 2 and experimental FT-IR spectrum of $C_{140}O(A)$.

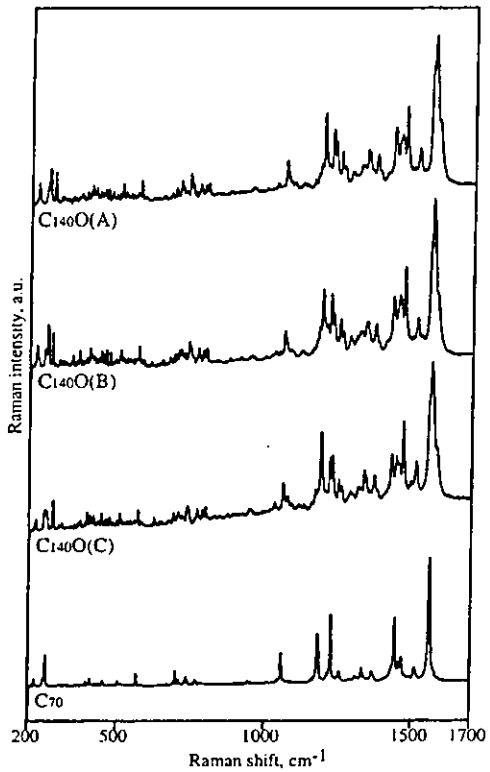

Figure 8. Raman spectra obtained by Ar ion laser excitation at 514.5 nm from isolated isomers of $C_{140}O$ (upper three spectra) and C_{70} (bottom).

and perhaps the interaction between the two C_{70} cages. The most remarkable difference between the isomers of $C_{140}O$ and C_{70} is the existence of peaks in the range from 1000 to 1150 cm^{-1}. Peaks in this range were considered to represent C−O−C vibration of dimeric fullerene oxide and were also observed in the IR spectra of $C_{120}O$ and $C_{130}O$.[5,9,10] This result suggested that $C_{140}O(A)$, (B), and (C) have the structure of conventional dimeric fullerene oxides, which are furan-bridged. The theoretical IR spectrum for $C_{140}O$ isomer 2 calculated with Hyperchem is shown in Figure 7 and exhibits a good agreement with experimental spectrum. In this theoretical spectrum, there are roughly three groups of lines: groups at around 600, 1100, and 1400 cm^{-1}. The group at 1100 cm^{-1} basically corresponds to C−O−C stretching modes of the furan connection between the C_{70} balls. The others are C−C modes within the C_{70} units. The group at around 600 cm^{-1} corresponds to radial motions, and the one at around 1100 cm^{-1} corresponds to the motions on the C_{70} surface. This calculation should also support the furan-bridged structure of $C_{140}O$ samples. Furthermore, the peak profile of $C_{140}O(B)$ in this C−O−C range seemed different from

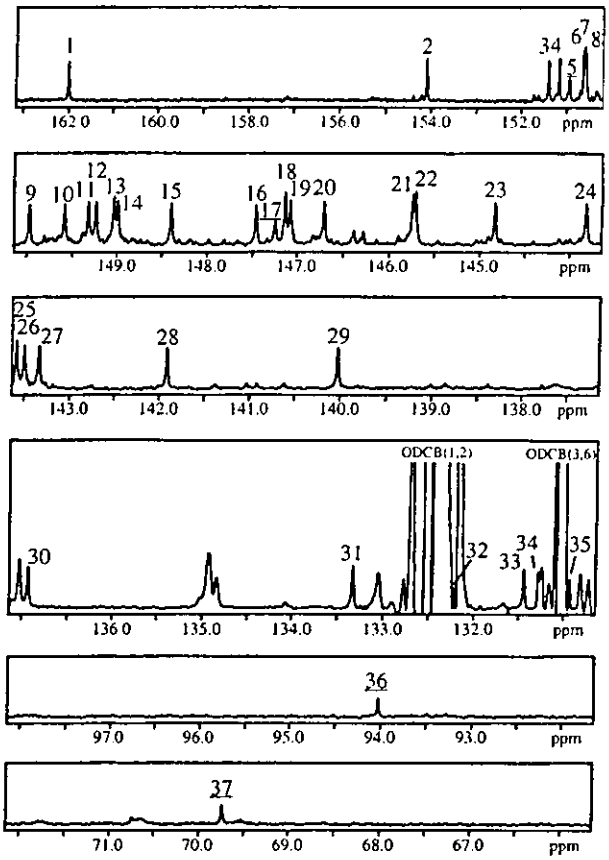

Figure 9. 125.76 MHz ^{13}C NMR spectrum of $C_{140}O(A)$ in o-dichlorobenzene-d4 with $Cr(acac)_3$ for paramagnetic relaxation enhancement. This sample was not enriched in ^{13}C. This spectrum was obtained with normal acquisition without 1H decoupling. Repetition time was 3 s and experimental time was 24 h. Peak assignment was done by comparing this spectrum and spin−echo spectrum.

that of $C_{140}O(A)$ and (C). This should be related to different C−O−C vibration modes in each isomer, caused by different junctions between two C_{70} cages. This may be used for the structure assignment of each isomer and will be discussed in section 4−1. In addition, split peaks of each isomer in the range of small wavenumber (500−1000 cm^{-1}) were different from each other. It is well known that IR spectra are related to the structure or the symmetry of substance. Therefore, these differences suggested that the structure of each sample was different.

Figure 8 shows Raman spectra of isolated isomers of $C_{140}O$. Showing a similar trend with FT-IR, peaks of $C_{140}O$ isomers in Raman spectra were shifted and split compared to that of C_{70}. In each spectrum, there were slight differences in the relative intensities of each peak, but not as large as observed in FT-IR spectra. In dimeric fullerene species, it was reported that new peaks related to intercage vibration modes[15−20] were observed in the region around 100 cm^{-1}. Therefore, the existence of peaks in this region could support the dimeric structure of our samples. However, we could not obtain reliable data because of bright lines of the Ar ion laser.

3−4. NMR Measurements.

The ^{13}C NMR spectrum of $C_{140}O(A)$ is shown in Figure 9, and assigned resonances (37 peaks) are numbered and listed in Table 1. This spectrum corresponded to a single isomer of $C_{140}O$. The presence of other dimeric species as impurities was discarded because of the absence of any peaks in the sp3 region

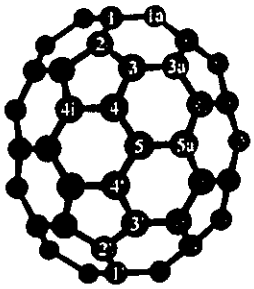

Figure 10. Structure of C_{70} with labeling to show the reaction site. The numbering is used to define the longitude and the letters a, b, c, etc. are used to define the latitude moving from west to east. Among eight possible reaction sites (1−1a, 1−2, 2−3, 3−3a, 3−4, 4−4i, 4−5, and 5−5a), the sites that have "formal double bond" are only 1−2 and 3−3a. 1−2 is called "polar" and 3−3a is called "tropical".

TABLE 1: ^{13}C NMR Data for $C_{140}O$(A) in ODCB-d4

no.	ppm	integral	no.	ppm	integral
1	162.32	4.00	20	147.03	4.04
2	154.4	3.92	21	146.06	4.32
3	151.71	3.88	22	146.03	4.76
4	151.47	4.12	23	145.16	3.96
5	151.25	1.92	24	144.14	4.56
6	150.94	4.60	25	143.92	4.68
7	150.91	3.88	26	143.83	4.68
8	150.91	4.44	27	143.67	4.68
9	150.29	3.92	28	142.25	3.84
10	149.91	4.08	29	140.36	4.04
11	149.7	4.44	30	137.26	4.20
12	149.56	4.64	31	133.66	4.08
13	149.36	5.00	32	132.54	0.76
14	149.31	4.20	33	131.77	3.44
15	148.72	4.20	34	131.61	2.40
16	147.78	3.84	35	131.26	1.52
17	147.57	2.52	36	94.36	1.60
18	147.46	5.68	37	70.07	1.88
19	147.4	4.84			

TABLE 2: ^{13}C NMR Data for $C_{140}O$(B) in ODCB-d4

ppm	I	ppm	I	ppm	I
162.90	1	148.21	1	144.26	1
161.96	1	148.15	1	144.23	1
157.46	1	147.80	1	144.06	1
155.65	1	147.74	3	143.96	1
154.84	1	147.61	1	143.91	1
154.47	1	147.58	3	143.89	1
154.16	1	147.53	2	143.83	1
152.03	1	147.47	1	143.74	1
152.01	1	147.42	1	143.35	1
151.85	1	147.27	2	142.66	1
151.62	3	147.22	1	142.24	1
151.39	1	147.14	1	142.01	1
151.06	3	147.11	1	141.82	1
150.96	1	146.92	1	141.16	1
150.89	1	146.83	1	140.66	1
150.75	1	146.78	1	140.31	1
150.69	1	146.67	1	137.20	1
150.36	1	146.52	1	137.13	1
150.20	2	146.38	1	133.86	1
150.10	1	146.33	1	133.66	1
150.02	1	146.27	2	132.37	1
150.00	1	146.21	1	132.00	1
149.91	1	146.19	1	131.77	1
149.80	1	146.16	1	131.75	1
149.78	1	146.07	1	131.65	1
149.74	1	146.04	2	131.53	1
149.73	1	145.93	1	131.38	1
149.66	1	145.45	1	131.34	1
149.58	1	145.44	1	131.15	1
149.50	1	145.27	1	130.94	1
149.45	3	145.18	1	130.99	1
149.41	1	145.16	1	130.14	1
149.36	1	144.94	1	130.09	1
149.33	1	144.78	1	126.96	1
150.31	1	144.69	2	125.83	1
149.28	1	144.53	1	94.79	1
149.23	1	144.48	1	90.59	1
148.88	1	144.44	1	72.95	1
148.82	3	144.38	1	67.99	1
148.58	1	144.36	1		
148.34	1	145.29	1		

of the spectrum except of the two peaks originated from $C_{140}O$(A). The numbers of NMR peaks for isomers 1 and 2 were predicted to be 37 by Fowler et al. (Figure 3).[14] Therefore, $C_{140}O$(A) was considered to be either isomer 1 or 2. The only difference between isomer 1 and 2 is the position of the oxygen atom. In isomer 1 and 2, the oxygen atoms are attached to carbon atom no. 1 and 2, respectively, as shown in Figure 10.

Figure 11 shows the ^{13}C NMR spectrum of $C_{140}O$(B), and 139 NMR peaks are numbered and listed in Table 2. Large solvent peaks are considered to hide one of 140 peaks. The peaks of one major isomer and minor isomer(s) were found from the spectrum. From the peak integrals, concentration of the minor isomer was estimated to be 10−15%, but it was impossible to count the number of peaks as most of them were hidden in the major peaks. In the theoretical prediction by Fowler et al., isomers that have 140 peaks were isomers 4 and 5. Similar to isomer 1 and 2, the only difference between isomers 4 and 5 was the position of oxygen atom.

Unfortunately, the S/N ratio of ^{13}C NMR spectrum of $C_{140}O$(C) was not high enough to count the number of peaks. This was due to low stability of $C_{140}O$(C), which precipitated in a few hours at the concentration necessary for NMR measurements. Nevertheless, we found that $C_{140}O$(C) has at least 60 NMR peaks.

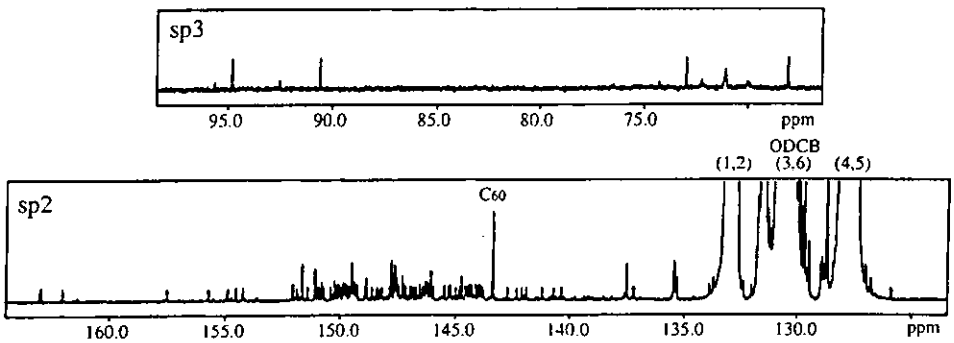

Figure 11. 125.76 MHz ^{13}C NMR spectrum of $C_{140}O$(B) in o-dichlorobenzene-d4 with $Cr(acac)_3$ for paramagnetic relaxation enhancement. Also, this sample was not enriched in ^{13}C. Repetition time was 3 s and experimental time was 56 h. Large peak at 143.29 ppm is attributed to C_{60} as contaminant.

4. Discussion

4−1. Structure of $C_{140}O$.

Theory predicts that $C_{140}O$ should have seven isomers (Figure 3). The formal double bonds in C_{70} are limited to its capping region and are classified into "polar" double bonds and "tropical" double bonds named in ref 14. The former radiates from the pentagon of the 5-fold axis, and the latter links the circuit of five pentagons. From the combination of these two formal double bonds, the alternative direction of C_{70} and the position of the oxygen atom, seven isomers are possible.

From the NMR measurements, it was clear that $C_{140}O$(A) should have the structure of isomer 1 or 2. Since isomer 1 and 2 have the same C_{2v} symmetry, it was difficult to distinguish one from the other even with Raman or IR spectra as much as NMR spectra. According to the MNDO calculation by Fowler et al., isomer 2 has a more favorable structure (see Figure 3; dEm (isomer 1) = 0.8, dEm (isomer 2) = 0.0). Energetically, the difference between them is marginal and it is risky to determine the structure only from theoretical calculations. Further, the theoretical calculation cannot explain the reason for the synthesis of only one of the isomers 1 or 2 (or 4 or 5) in large quantity. By the way, Lebedkin et al.[15] has already succeeded in the synthesis, isolation, and structural determination of dimeric C_{70}, that is, C_{140}. They also considered two structures from the result of NMR measurements. Nevertheless, they succeeded in the structural determination from the well-known structure of C_{70} crystal. In our case, structural determination was very difficult as there is no structural information on C_{70}/$C_{70}O_n$ mixed crystals available.

Here, we propose the possible structural assignment based on the position of the oxygen atom in $C_{140}O$. As a matter of fact, $C_{70}O$ is needed for the synthesis of $C_{140}O$. Only two types of $C_{70}O$ can be synthesized with almost equal yield.[21−23] One of them is of (1,2) type and the other is of (3,3a) type (see Figure 10). According to several theoretical calculations,[24,25] the most stable isomer of $C_{70}O$ is (5,5a) type, though the reason is unclear. The (1,2) and (3,3a) type isomers are produced during synthesis. For the synthesis of $C_{140}O$, one of two C−O bonds in $C_{70}O$ should be broken. But in the case of (3,3a) type, these two bonds are symmetrical and equivalent to each other. Thus, the selectivity of the breaking bond does not affect the subsequent structure of $C_{140}O$. On the other hand, the (1,2) type also has two C−O bonds; however, they are not equivalent. In our semiempirical PM3 calculations using CS MOPAC software equipped in CS ChemBats3D Pro, the bond lengths do not show a clear difference (0.1424 nm for C(1)−O bond and 0.1425 nm for C(2)−O bond). However, the Mulliken charges are different, 0.08485e for C(1) and 0.07571e for C(2). Also in other calculation methods such as AM1 and MNDO, the charge of C(1) is higher than that of C(2) though the absolute values are different from the PM3 method. In the synthesis of dimeric fullerene oxides through hydrothermal treatment, the formation of dimeric fullerene oxides has been proposed through the nucleophilic addition reaction. As it is well known, nucleophile (in our case, OH^- ions) attacks preferentially the positively charged portion of the molecule in the above reaction. Therefore, we believe that OH^- ion tends to attack the C(1) atom, which has higher charge, and to break the C(1)−O bond rather than the C(2)−O bond. Taking this into account, we propose that $C_{140}O$(A) contains the structure of isomer 2.

Also for $C_{140}O$(B), two structures were considered from NMR measurements. Complete structural assignment was impossible for the same reason as in $C_{140}O$(A). Nevertheless, we suppose that the structure of $C_{140}O$(B) corresponds to isomer 4 for the reason mentioned above. However, this assignment does not match with the energetic calculation by Fowler et al.[14] The energetic difference between isomer 4 (dEm = 3.9) and isomer 5 (dEm = 3.5) is marginal. Isomer 4 and 5 could be formed from (3,3a) type $C_{70}O$ that has symmetrical C−O bonds. Therefore, on the basis of simple calculation, the ratio of yields between isomers 4 and 5 should be 3:1. This calculation is under the hypothesis that equal amounts of (1,2) type $C_{70}O$ and (3,3a) type $C_{70}O$ are included in the starting material, (1,2) type $C_{70}O$ yields isomer 4 only, and (3,3a) type $C_{70}O$ yields both isomer 4 and 5 in equal efficiency. In this study, only the species marked with A, B, and C in Figure 2 were isolated and investigated. It thus appears that isomer 5 was not found; however, we believe that it should exist in the sample after hydrothermal treatment.

Unfortunately, the ^{13}C NMR spectrum of $C_{140}O$(C) could not be obtained with high S/N ratio. Therefore, perfect structural determination of $C_{140}O$(C) was impossible. However, we can propose the structure by interpreting FT-IR spectra. In the C−O−C vibration region, $C_{140}O$(A) and (C) have similar profiles with three major peaks and three minor peaks, but $C_{140}O$(B) was different and free of minor peaks. These differences were considered because of the difference in the junction between two C_{70} cages. In $C_{140}O$(A), namely, isomer 2 (or 1), the junction can be described as (1,2)/(1,2) [or (2,1)/(2,1)]. On the other hand, in $C_{140}O$(B) (isomer 4 or 5), the junction can be described as (1,2)/(3,3a) or (2,1)/(3,3a). Therefore, the split of peaks in $C_{140}O$(A) and (C) in the C−O−C vibration region could be attributed to the junction at the (1,2) site in C_{70}. These types of junction have relatively higher symmetry. Among all seven isomers, the ones that have the above junction were isomers 1, 2, and 3. The number of NMR peaks for both isomer 1 and 2 is 37. As mentioned above, at least 60 NMR peaks were found in the spectrum of $C_{140}O$(C). This suggests that $C_{140}O$(C) could not have the structure of isomer 1 or 2. From this elimination method, we believe that $C_{140}O$(C) has the structure of isomer 3. This unstable isomer was predicted to be relatively stable in the theoretical calculation by Fowler et al.[14] Unfortunately, we cannot provide a clear interpretation for this discrepancy, but the predictions of Fowler et al. for various dimeric fullerene oxide species were usually confirmed by experiment.

In summary, the ^{13}C NMR measurements provides firm evidence that (1) $C_{140}O$(A) corresponds to the structure of isomer 1 or 2 and (2) $C_{140}O$(B) corresponds to the structure of isomer 4 or 5. On the other hand, from PM3 calculation for Mulliken charge distribution and from FT-IR measurements, we concluded that $C_{140}O$(A) and (B) correspond to the structure of isomers 2 and 4, respectively. Furthermore, $C_{140}O$(C) has the structure of isomer 3.

4−2. Alternative Method for the Synthesis of $C_{140}O$.

In this paper, we used the hydrothermal treatment for the synthesis of dimeric fullerene oxides. However, several other methods have been already reported for the synthesis of dimeric fullerene oxides.[5,7] Among them, we attempted Lebedkin's method where C_{60}/$C_{60}O$ mixed powder is heated to 473 K in an Ar atmosphere.[5] At first, the C_{70}/$C_{70}O_n$ starting material was heated to 473 K under similar experimental condition as in the case of $C_{120}O$. From the resulting substance, HPLC and mass peaks of $C_{140}O$ were observed. However, a large part of substance was insoluble in both toluene and o-dichlorobenzene. Mass analysis suggested the substance to be polymeric C_{70} oxides, and the reaction temperature of 473 K was considered to be too high for C_{70} species. From the analysis of the products

synthesized at various temperatures, the optimum temperature for the synthesis of $C_{140}O$ was considered to be 423 K. Though the yield of $C_{140}O$ synthesized under this condition was slightly higher than the hydrothermal method, the yield of insoluble species was comparatively high. C_{70} is not so an abundant fullerene as C_{60} and also, the efficient conversion of polymeric fullerene oxide species to its monomer is not known to date. Therefore, we believe that our hydrothermal treatment is the most suitable method for the synthesis of $C_{140}O$ from the viewpoint of recycling unreacted C_{70}.

5. Summary

We have shown that $C_{140}O$ could be synthesized in large quantity by the hydrothermal method which was used for the synthesis of $C_{120}O$. From summing the area of newly observed HPLC peaks, the yield was estimated to be 2−3%. $C_{140}O$ can also be synthesized with Lebedkin's heating method. However, in this method, besides $C_{140}O$, insoluble polymeric species were also synthesized in large quantities. From the viewpoint of recycling unreacted C_{70}, the hydrothermal treatment was preferred over the heating method. HPLC charts and mass spectra showed the existence of polyoxides and the isomers of $C_{140}O$ as predicted by Fowler et al. Three isomers were isolated by HPLC and investigated by MALDI-TOF-MS, UV−Vis, FT-IR, and Raman. These results showed the similarity between $C_{140}O$ and $C_{120}O$ and support that our $C_{140}O$ samples have the structure of conventional furan-bridged dimer.

^{13}C NMR measurements showed that the structure of $C_{140}O(A)$ was the one of isomer 1 or 2 and that the structure of $C_{140}O(B)$ was the one of isomer 4 or 5. Complete assignments of structures were impossible; however, we suppose that the structure of $C_{140}O(A)$ and (B) should be assigned to isomer 2 and 4, respectively, from Mulliken charge calculation. For $C_{140}O(C)$, we suppose it to have the structure of isomer 3 from the elimination method.

Acknowledgment. The present study was supported in part by Grant-in-Aid for Priority Research (#11165202) and International Scientific Research Program (#11694119) from the Ministry of Education, Science, Culture, and Sports of Japan and CREST of Japan Science and Technology Institute. The authors thank Mrs. Ruth Alberts for the technical support in the synthesis of $C_{140}O$, Dr. Sergei Lebedkin for the advice about HPLC retention time, Dr. Jürgen Gross for the advice in MALDI measurements, Dr. Kenji Kodama and Dr. Yoko Miyake for valuable discussion about NMR measurements, and Dr. Takatoshi Matsumoto for the advice in using Mulliken charge calculations.

References and Notes

(1) McElvany, S. W.; Callahan, J. H.; Ross, M. M.; Lamb, L. D.; Huffman, D. R. *Science* **1993**, *260*, 1632.

(2) Deng, J. P.; Ju, D. D.; Her, G. R.; Mou, C. Y.; Chen, C. J.; Lin, Y. Y.; Han, C. C. *J. Phys. Chem.* **1993**, *97*, 11575.

(3) Beck, R. D.; Brauchel, G.; Stoermer, C.; Kappes, M. M. J. *Chem. Phys.* **1995**, *102*, 540.

(4) Taylor, R. J. *Chem. Soc., Chem. Commun.* **1994**, 1629.

(5) Lebedkin, S.; Ballenweg, S.; Gross, J.; Taylor, R.; Krätschmer, W. *Tetrahedron Lett.* **1995**, *36*, 4971.

(6) Gromov, A.; Lebedkin, S.; Ballenweg, S.; Krätschmer, W. *Fullerenes and Fullerene Nanostructure. Proceedings of the International Winterschool on Electronic Properties of Novel Materials*; Kuzmany, H., Fink, J., Mehring, M., Roth, S., Eds.; World Scientific: Singapore, 1996; p 460.

(7) Smith, A. B.; Tokuyama, H.; Strongin, R. M.; Furst, G. T.; Romanow, W. J. *J. Am. Chem. Soc.* **1995**, *117*, 9359.

(8) Gromov, A.; Ballenweg, S.; Giessa, S.; Lebedkin, S.; Hull, W. E.; Krätschmer, W. *Chem. Phys. Lett.* **1997**, *267*, 460.

(9) Kudo, T.; Takahashi, H.; Shinoda, K.; Jeyadevan, B.; Tohji, K.; Nirasawa, T.; Kasuya, A.; Nishina, Y.; Krätschmer, W. *Recent Research Developments in Physical Chemistry* **2001**, *5*, 301. Takahashi, H.; Matsubara, E.; Kasuya, A.; Akimoto, Y.; Kudo, T.; Jeyadevan, B.; Tohji, K. *Proc. Int. Symp. on Cluster Assembled Mater. IPAP Conf.* **2001**, *3*, 118.

(10) Deng, J. P.; Mou, C. Y.; Han, C. C. *Chem. Phys. Lett.* **1996**, *256*, 96.

(11) Al-Jafari, M. S.; Barrow, M. P.; Taylor, R.; Drewello, T. *Int. J. Mass Spectrom.* **1999**, *184*, L1.

(12) Wang, G. W.; Komatsu, K.; Murata, Y.; Shiro, M. *Nature* **1997**, *387*, 583.

(13) Akimoto, Y.; Kudo, T.; Shinoda, K.; Jeyadevan, B.; Tohji, K.; Nirasawa, T.; Kasuya, A.; Nishina, Y. *Proc. Int. Symp. on Cluster Assembled Mater. IPAP Conf.* **2001**, *3*, 123.

(14) Fowler, P. W.; Michell, D.; Taylor, R.; Seifert, G. *J. Chem. Soc., Perkin Trans. 2* **1997**, 1901.

(15) Lebedkin, S.; Hull, W. E.; Soldatov, A.; Renker, B.; Kappes, M. M. *J. Phys. Chem. B* **2000**, *104*, 4101.

(16) Eisler, H. J.; Hennrich, F. H.; Werner, E.; Hertwig, A.; Stoermer, C.; Kappes, M. M. *J. Phys. Chem.* **1998**, *A102*, 3889.

(17) Adams, G. B.; Page, J. B.; Sankey, O. F.; O'Keeffe, M. *Phys. Rev.* **1994**, *B50*, 17471.

(18) Porezag, D.; Pederson, M. R.; Frauenheim, T.; Kpöhler, T. *Phys. Rev.* **1995**, *B52*, 14963.

(19) Krause, M.; Dunsch, L.; Seifert, G.; Fowler, P. W.; Gromov, A.; Krätschmer, W.; Gutierez, R.; Porezag, D.; Frauenheim, T. *J. Chem. Soc. Faraday Trans.* **1998**, *94*, 2287.

(20) Lebedkin, S.; Gromov, A.; Giesa, S.; Gleiter, R.; Renker, B.; Rietschel, H.; Krätschmer, W. *Chem. Phys. Lett.* **1998**, *285*, 210.

(21) Bezmelnitsin, V. N.; Eletskii, A. V.; Schepetov, N. G.; Avent, A. G.; Taylor, R. *J. Chem. Soc., Perkin Trans. 2* **1997**, 683.

(22) Balch, A. L.; Costa, D. A.; Olmsted M. M. *Chem. Commun.* **1996**, 2449.

(23) Smith, A. B.; Strongin, R. M.; Brard, L.; Furst, G. T.; Atkins, J. H.; Romanow, W. J. *J. Org. Chem.* **1996**, *61*, 1904.

(24) Raghavachari, K. *Chem. Phys. Lett.* **1992**, *197*, 4, 5, 495.

(25) Wang, B. C.; Chen, L.; Chou, Y. M. *J. Mol. Struct. (THEOCHEM)* **1998**, *422*, 153.

Jpn. J. Appl. Phys. Vol. 42 (2003) pp. L350–L352
Part 2, No. 4A, 1 April 2003

Express Letter

Direct Synthesis of fct-FePt Nanoparticles by Chemical Route

Balachandran JEYADEVAN, Kiyoshi URAKAWA, Akira HOBO, Nallasamy CHINNASAMY, Kozo SHINODA, Kazuyuki TOHJI, David D. Julianto DJAYAPRAWIRA[1], Masakiyo TSUNODA[1] and Migaku TAKAHASHI[1]

Department of Geoscience and Technology, Tohoku University, Aoba-ku, Sendai 980-8579, Japan
[1]*Department of Electronic Engineering, Tohoku University, Aoba-ku, Sendai 980-8579, Japan*

(Received February 18, 2003; accepted for publication February 25, 2003)

Direct synthesis of fct-FePt nanoparticles was achieved by reducing platinum and iron acetylacetonates in tetraethylene glycol (TEG) at 300°C. The particle diameter was between 5 and 10 nm. The X-ray diffraction profile of the as-prepared FePt particles exhibited the superlattice reflections (001) and (110), which signified the tetragonality. The H_k of 31 kOe measured at room temperature (RT) from hysteresis loss analysis confirmed the presence of FePt particles with fractionally ordered fct structure which posses substantially high anisotropy. However, the RT coercivity was only 370 Oe due to strong magnetostatic interaction of the particles. [DOI: 10.1143/JJAP.42.L350]

KEYWORDS: FePt, nanoparticles, fct-FePt, $L1_0$ phase, super lattice reflections, polyol process, direct synthesis, coercive field, hysteresis loss analysis

Considerable interest is being shown towards the chemical synthesis of self-assembled, monodispersed and chemically ordered $L1_0$ FePt and CoPt nanoparticles for the new generation ultra density magnetic storage.[1–4] The ordered $L1_0$ phase of these systems posses high magnetocrystalline anisotropy (K_u) and allows the use of thermally stable particles with 4–5 nm in diameter[5] as the basic unit for recording. The as-synthesized particles are reported to be superparamagnetic, chemically disordered and fcc in structure.[1] To obtain the $L1_0$ structure, the particles need to undergo annealing at temperature as high as 580°C. However, annealing leads to the coalescence of nano particles and restricts high-density recording. Therefore, both from fabrication and grain growth perspective, it is important to lower the phase transition temperature (T_t). Reasonable success has been achieved by adding a third element (*e.g.* Cu, Sn, Pb, Sb, Ag and Bi) that lower the T_t through surface segregation.[6,7] However, the reduction of T_t by above means has been limited and lowering below 400°C still remains a challenge. In nanoparticles, surface energy that constitutes large part of the total free energy can be a significant factor in structure determination. In addition to thermodynamic effects, reaction kinetics can be strongly size dependent. Furthermore, the activation barriers to phase transformations are relatively low in these very small particles.[8] This phenomenon gives rise to complex coupled growth-phase transformation behavior. For example, the bulk cobalt is known to have fcc phase at temperatures as high as 421.5°C. Authors in synthesizing cobalt metal particles using the chemical route, namely modified polyol process,[9–12] obtained the following: the particles chemically synthesized at temperatures as low as 195°C were found to posses fcc structure at micron size levels. When the reaction kinetics was enhanced, the particle size was reduced to submicron and even to few tens of nanometer. Along with size reduction, the crystal structure also changed from fcc at micron size range, coexistence of fcc and hcp in the submicron size range and to epsilon and hcp cobalt at nanometer size range.[9] The size reduction is a consequence of fast reaction kinetics and so the formation of unstable phases. Hence, we believed that during synthesis, the nanoparticles seem to undergo the formation of unstable phases and depending on the reaction kinetics, different particle sizes and crystal structures can be realized. On the other hand, if the reaction rate is slow, the formation of most stable phase is realized.

In the case of FePt synthesis by using polyol process, Fe as well as Pt ions has to be co-reduced. On the contrary to Co case, the reduction of Fe alone is considered difficult in polyol.[10] However, as observed in the case of Co particle synthesis, Pt ions not only reduced to Pt metal, but also induced and accelerated the reduction of associated metal ions.[9] Similar phenomena can be expected in the case of Fe ions, and could lead to the formation of FePt alloy particles using the polyol process alone rather than a combination of processes.[1] The FePt particles synthesized via chemical route are reported to be superparamagnetic and chemically disordered fcc structure.[1,4] The ordered fct structure is the stable phase and the chemically disordered fcc structure of as-synthesized particles is thought to be a consequence of the fast reaction kinetics. Therefore, it is believed that direct synthesis of chemically ordered fct structure is possible through finer control of the reaction kinetics.

The synthesis experiments were carried out using Fe and Pt acetylacetonates. The standard synthesis procedure is as follows: First, specified amounts of Fe and Pt salts were dissolved in 100 m*l* of glycol. Then, the solution was transferred to a vessel with reflux attachment and placed in an oil-bath and heated at a constant rate under gentle mechanical stirring. Typically, the suspension was refluxed at 195°C for three and a half hours to obtain FePt particles.

The particle morphology, composition, structure, and phase transition temperature (T_t) of as-prepared FePt particles were analyzed using high-resolution transmission electron microscopy (HRTEM-Hitachi HF 2000), energy dispersive X-ray spectroscopy (TEM-EDX), X-ray diffraction (XRD) (Rigaku-Cu-K_α radiation), and differential scanning calorimetry (DSC) (Rigaku DSC 8270) in N_2 atmosphere from 50 to 700°C at a heating rate of 20 K/min, respectively. The magnetization (M_s) and coercivity (H_c) of unoriented assemblies of the nanoparticles were measured using magnetic property measurement system superconducting quantum interference devices (MPMS SQUID) with maximum applied field of 5 T. The rotational hysteresis loss was measured at room temperture (RT) by using a highly sensitive torque magnetometer (Tamakawa, Japan) with

magnetic field up to 25 kOe.

Depending on Fe and Pt acetylacetonate molar ratio, particles diameter of about 4 nm and the composition of Fe ranging between 40 and 60 at% was obtained. Furthermore, the XRD pattern revealed that the as-synthesized particles were of chemically disordered fcc structure and the average grain size was 3–4 nm in diameter. However, by manipulating the reaction parameters such as, types of polyol, reaction temperature and metal ion concentration (Polyol/Pt mole ratio), on the premises that slow kinetics of the reaction would give ordered FePt particles, we succeeded in synthesizing partially ordered ferromagnetic FePt particles with low T_t[2]. Especially the T_t of FePt particles was found to be very sensitive to the metal ion concentration (polyol/Pt mole ratio). Under the optimum experimental condition in EG, the T_t was reduced to about 300°C.

Attempting the synthesis of fct-FePt particles directly, experiments were carried out in TEG whose boiling point (327°C) is higher than the T_t of the particles synthesized in EG. The T_t of the FePt particles synthesized at 260°C was around 280°C and suggested the possibility of structural transformation during synthesis at temperatures above 280°C in TEG. XRD patterns of as-synthesized FePt particles in TEG at 260°C [sample (a)] and 300°C [sample (b)] are shown in Fig. 1. The presence of diffraction peaks corresponding to the superlattice reflections (001) and (110) in the XRD profile of sample (b) confirmed the tetragonality. The particle diameter varied between 5 and 10 nm depending on the reaction temperature and time and the particle synthesized at 300°C is given in Fig. 2.

To confirm the presence of the ordered fct phase, the intrinsic magnitude of uniaxial magnetic anisotropy field H_k of the above sample was evaluated using rotational hysteresis loss anaysis method, which is reliable and well established to determine the H_k of hard-disk media.[13] Figure 3 shows the rotational hysteresis loss W_r plotted as a function of applied magnetic field H for samples (a) and (b). Here, H_k was defined as the magnetic field obtained by extrapolating the linear part of W_r curve at high fields to $W_r = 0$. H_k for the sample (a) was only 3.7 kOe. However, the sample (b) that was synthesized in TEG at 300°C showed a value of 31 kOe. Although the H_k of a perfectly ordered $L1_0$ FePt is reported to be as high as 116 kOe,[5] the result confirmed the presence of FePt particles with fractionally ordered fct structure which posses substantially high anisotropy.

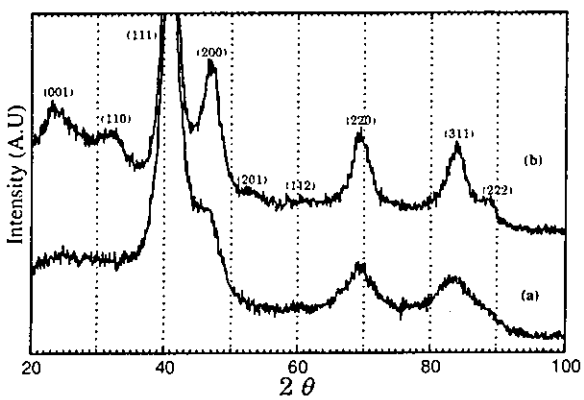

Fig. 1. X-ray diffraction patterns of as-synthesized FePt particles in TEG at (a) 260°C and (b) 300°C.

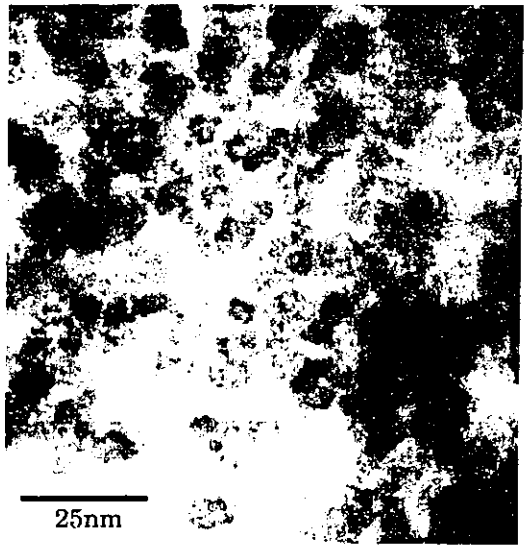

Fig. 2. The TEM micrograph of FePt particles synthesized at 300°C in TEG.

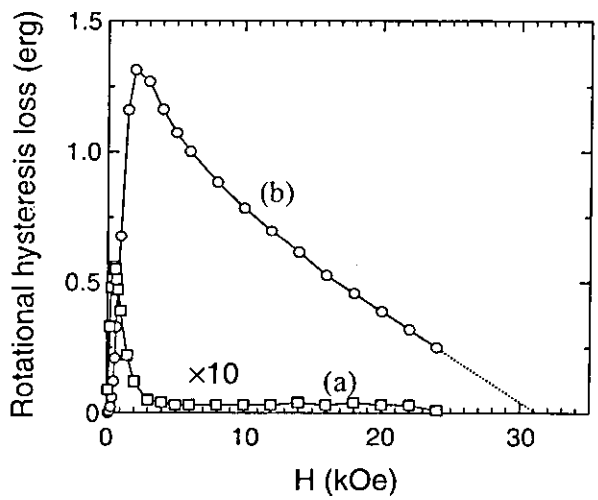

Fig. 3. The rotational hysteresis loss W_r plotted as a function of applied magnetic field H for samples synthesized in TEG at (a) 260°C and (b) 300°C.

The magnetic hysteresis loops of samples (a) and (b) are shown in Fig. 4. Though the saturation magnetization was found to be as high as 40 emu/g, the coercivity at room temperature of the powder synthesized at 300°C was merely 370 Oe, in spite of the presence of fct phase. This was believed due to strong magnetostatic interaction between particles. The δM plot of sample (b) showed a negative maximum suggesting magnetostatic interaction between particles. Considering the fact that the degree of magnetostatic interaction is proportional to the cube of the inverse of grain size, and the grain size of the FePt samples were very small, the magnetostatic interaction is suggested to be very strong.

Furthermore, from the above magnetic measurements, K_u of sample (b) was evaluated to be 1.45×10^7 erg/cc. Thus,

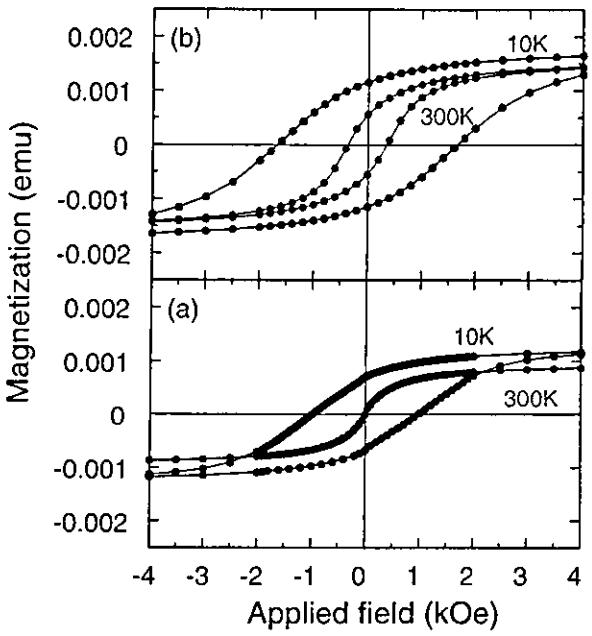

Fig. 4. Hysteresis loops of as-synthesized FePt particles in TEG at (a) 260°C and (b) 300°C.

assuming the particle to be 7.5 nm in diameter, the KV/kT will be around 80. This infers that the low coercivity is not due to superparamagnetism, but due to strong particle interaction. This is supported by the fact that the coercivity of the particle at 10 K was only about 1.7 kOe. Thus, the particles have to be dispersed for the application of the same in magnetic recording. The work is in progress to achieve the same. A detailed report on the synthesis technique and the magnetic properties of particles prepared under different synthesis conditions will be reported elsewhere.

We conclude that the control of the reaction kinetics results in the reduction of T_t in FePt particles. Platinum ion concentration in the polyol was found to be one of the parameters that retarded the reaction kinetics of the reduction process very effectively. The FePt particles prepared under optimum condition were 5–10 nm in diameter with considerable fraction of fct phase with an anisotropy field of 31 kOe at RT. The direct synthesis of fct-FePt particles would revive the interest and efforts towards achieving high recording densities and in excess of 1 Tb/in^2 will be realized in the near future.

The authors wish to thank Mr. Kenichi Motomiya for his kind assistance in TEM and HRTEM analysis. This study was supported by Grant-in-Aid for Basic Research #(S) 14103016, and #(S) 13852016 from the Ministry of Education, Science, Culture and Sport of Japan and # H14-nano-021 from the Ministry of Health, Labor and Welfare.

1) S. Sun, C. B. Murray, D. Weller, L. Folks and A. Moser: Science **287** (2000) 1989.
2) B. Jeyadevan, A. Hobo, K. Urakawa, C. N. Chinnasamy, K. Shinoda and K. Tohji: to be published in J. Appl. Phys. (2003).
3) C. N. Chinnasamy, B. Jeyadevan, K. Shinoda and K. Tohji: to be published in J. Appl. Phys. (2003).
4) M. Chen and D. E. Nikles: J. Appl. Phys. **91** (2002) 8477.
5) D. Weller, A. Moser, L. Folks, M. E. Best, W. Le, M. F. Toney, M. Schwickert, J. U. Thiele and M. F. Doerner: IEEE Trans. Magn. **36** (2000) 10.
6) O. Kitakami, Y. Shimada, K. Oikawa, H. Daimon and F. Fukamichi: Appl. Phys. Lett. **78** (2001) 1104.
7) S. Kang, J. W. Harrell and D. E. Nikles: Nano Lett. **2** (2002) 1033.
8) A. A. Gribbs and J. F. Banfield: Am. Mine. **82** (1997) 717.
9) B. Jeyadevan, O. P. Perez, C. N. Chinnasamy, K. Shinoda, K. Tohji and A. Kasuya: Dig. 26th Annual Conf. Magnetics in Japan 2002, Tokyo, p. 36.
10) G. Viau, F. Fievet-Vincent and F. Fievet: J. Mater. Chem. **6** (1996) 1047.
11) O. Perales-Perez, B. Jeyadevan, N. Chinnasamy, K. Tohji and A. Kasuya: *Proc. Int. Symp. Cluster Assembled Materials, Nagoya, 2001* (IPAP, Tokyo, 2001) IPAP Conf. Ser. Vol. 3, p. 105.
12) B. Jeyadevan, O. P. Perez, C. N. Chinnasamy, K. Shinoda and K. Tohji: *MMIJ Meet.* (2002) 133.
13) M. Takahashi, T. Shimatsu, M. Suekane, M. Miyamura, K. Yamaguchi and H. Yamasaki: IEEE Trans. Magn. **28** (1992) 3285.

Towards direct synthesis of fct-FePt nanoparticles by chemical route

B. Jeyadevan,[a] A. Hobo, K. Urakawa, C. N. Chinnasamy, K. Shinoda, and K. Tohji
Department of Geoscience and Technology, Tohoku University, Sendai, 980-8579, Japan

(Presented on 14 November 2002)

The possibility for direct synthesis of fct-FePt nanoparticles of the order of 3–4 nm in diameter through the coreduction of iron and platinum ions in a polyol has been explored. We have succeeded in the synthesis of face-centered cubic structured 3–4 nm diameter FePt particles whose composition was very close to $Fe_{50}Pt_{50}$. The Fe:Pt ratio was influenced little by the molar ratios of Fe and Pt acetylacetonate dissolved in ethylene glycol. However, depending on the polyol/Pt ratio, the as-prepared samples were either superparamagnetic or ferromagnetic. The transition temperature (T_t) and magnetic properties of the as-prepared FePt were very sensitive to the reaction conditions, and the T_t varied between 593 and 893 K and the particles were ferromagnetic. The as-prepared FePt under the optimum condition had a T_t as low as 593 K and H_c as high as 1.11 kOe at an applied field of 1 T at room temperature. Furthermore, when the as-prepared FePt nanoparticles with T_t around 593 K were annealed at 673 K in H_2/N_2 atmosphere for an hour they transformed to the ordered fct ($L1_0$) structure with coercivity as high as 4.2 kOe at 300 K. This confirmed the lowering of T_t by the manipulation of the reaction condition alone. © *2003 American Institute of Physics.*
[DOI: 10.1063/1.1558258]

I. INTRODUCTION

For high-density recording in thin film, magnetic grains must be small, uniform in size, and isolated to reduce media noise. Thus, only material that possesses large uniaxial anisotropy (K_u) can resist thermal fluctuations. For this, chemically ordered FePt with $L1_0$ structure that possesses one of the highest K_u (about 10^8 erg/cm^3), moderate magnetic moment and good corrosion resistance has been considered. This opens up the possibility of storing one data bit in a single tiny 3–4 nm diameter magnetic grain, and this has been already demonstrated.[1] However, the as-prepared FePt particles were superparamagnetic and have the face-centered cubic (fcc) structure. These particles have to be annealed at temperatures as high as 853 K to make the platinum and iron atoms transform into the face-centered tetragonal (fct) structure and retain magnetic orientation to be useful for recording. This annealing step has been found to promote the sintering of the ultra fine particles and hinder their performance as high-density recording material. This has prompted researchers to look for ways to reduce T_t of FePt from disordered to ordered state. Researchers have suggested the addition of a third element (e.g., Cu, Sn, Pb, Sb, and Bi) to lower the T_t through surface seggregation.[2,3] In this article, we report the synthesis of fcc-FePt nanoparticles of the order of 3–4 nm in diameter by using the polyol process. Also, we discuss the possibility for direct synthesis of fct-FePt particles by controlling the reaction kinetics of the chemical process.

II. EXPERIMENT

A. Synthesis of FePt particles

The synthesis experiments were carried out using Fe acetylacetonate and Pt complexes without any further purification. The standard synthesis procedure is as follows: First, specified amounts of Fe and Pt salts were dissolved in 100 ml of ethylene glycol. Then, the solution was transferred to a vessel with reflux attachment and placed in an oil-bath and heated at a constant rate under gentle mechanical stirring. During this stage, generally, the pale yellow colored solution turned colorless and finally black suggesting the formation of FePt particles. Typically, the suspension was refluxed at 468 K for three and one half hours.

B. Characterization

The phases produced in as-prepared FePt particles were analyzed using x-ray diffraction (XRD) (Rigaku—Cu $K\alpha$ radiaion). The morphology of the particles was examined by direct observation via high-resolution transmission electron microscopy (HRTEM-Hitachi HF 2000). The composition of the as-prepared FePt nanoparticles was determined by energy dispersive x-ray spectroscopy. The specific magnetization (M_s) and coercivity (H_c) of unoriented assemblies of the prepared powders were measured at room temperature (RT) in a maximum applied field of 15 T using a vibrating sample magnetometer (VSM Tamakawa model TM-VSM1230-HHHS). The phase transition temperatures of the particles were determined using a differential scanning calorimetry (DSC) (Rigaku DSC-8270) in a N_2 atmosphere.

III. RESULTS AND DISCUSSION

The polyol process has been used for the synthesis of different types of metal particles with diameters of the order

[a]Electronic mail: jeya@ni4.earth.tohoku.ac.jp

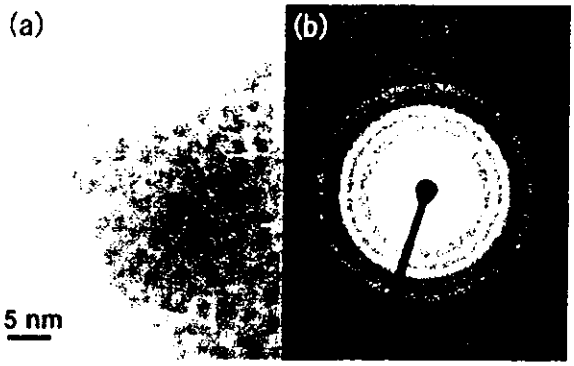

FIG. 1. The (a) TEM micrograph and (b) electron diffraction of the FePt particles synthesized in ethylene glycol.

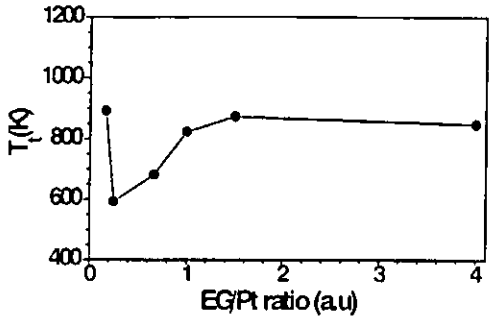

FIG. 2. Relation between Pt concentration and transformation temperature (T_t) of FePt particles synthesized in ethylene glycol.

of micron to submicron.[4] The authors have been working on transition-metal particles and succeeded in the synthesis of Co and Ni particles with diameters as small as a few tens of nanometers.[5] Furthermore, in the case of Co particles, a method was formulated to synthesize different crystal structures by controlling the reaction kinetics of the reduction reaction in polyol.[6] As a result, it was confirmed that by increasing the reaction kinetics, unstable crystal structures such as ε-Co and hcp-Co were formed. As opposed to the Co case, the reduction of Fe is considered impossible in polyol. However, as observed in the case of Co particle synthesis, Pt ions not only reduce to Pt metal, but also induce and accelerates the reduction of associated metal ions.[6] Similar phenomena can be expected in the case of Fe ions, and could lead to the formation of FePt alloy particles using the polyol process alone rather than a combination of processes.[1] It should be noted that the selection of the Pt complex is another important factor in the synthesis of Pt-based alloys. The synthesis of FePt was attempted with various Pt complexes. A Pt complex with a labile ligand such as hexachloroplatinate does not form FePt. However, when Pt acetylacetonate was reduced in the presence of Fe acetylacetonate in ethylene glycol, FePt particles were formed. It is believed that the kinetics of Pt reduction reaction plays a vital role in the synthesis of FePt. FePt alloys are known to form fcc solid solution over almost the whole concentration range. Around the equiatomic composition, annealing at comparatively low temperatures induces a transition from fcc to fct. Irrespective of Fe and Pt acetylacetonate molar ratio dissolved in ethylene glycol the composition of Fe ranged between 40 and 50 at. % with particle diameter about 3–4 nm as shown in Fig. 1(a). The electron diffraction pattern of the FePt particles is shown in Fig. 1(b). Furthermore, the XRD pattern revealed that the as-synthesized particles are of chemically disordered fcc structure and the average grain size was found to be 5 nm. The authors believe that the disordered structure is a consequence of fast kinetics of the reaction during synthesis. The present experimental conditions are favorable to induce a reduction reaction rate fast enough to cause atomic disorder in the crystal structure. If this can be controlled, the possibility of obtaining an ordered structure becomes higher. Based on these premises, the polyol/Fe ratio was decreased as a means to retard the reduction reaction. In other words, the concentration of Pt ions was varied. The transition temperatures of the products were determined by carrying out DSC studies from 50 to 973 K at a heating rate of 20 K/min. The properties of FePt particles such as T_t of the products were very sensitive to the polyol/Fe ratio as shown in Fig. 2. Though a correlation between T_t and H_c was observed, more experiments are needed to confirm the same. However, at some optimum Pt ion concentration the T_t was as low as 593 K, and the as-prepared FePt nanoparticles were ferromagnetic with H_c of 1.11 kOe in an applied field of 1 T. To confirm the reduction in T_t, two samples with T_t of 657 and 825 K were annealed at 673 K for three hours. The coercivity enhancement of the two samples is shown in Fig. 3. The coercivity of the sample that had the T_t of 657 K increased from 153 to 1190 Oe, whereas the sample with T_t of 825 K increased from 106 to only 304 Oe in an applied field of 1 T. Figure 4 shows the hysteresis loops of the sample with T_t of 593 K for (a) as-prepared and (b) annealed at 673 K in H_2/N_2 atmosphere for an hour. It should be noted that annealing at temperatures as low as 673 K even without the addition of a third element transformed the particles to the ordered fct ($L1_0$) structure with coercivity as high as 4.2 kOe at RT. This confirmed the reduction in T_t between samples prepared at varying Pt ion concentra-

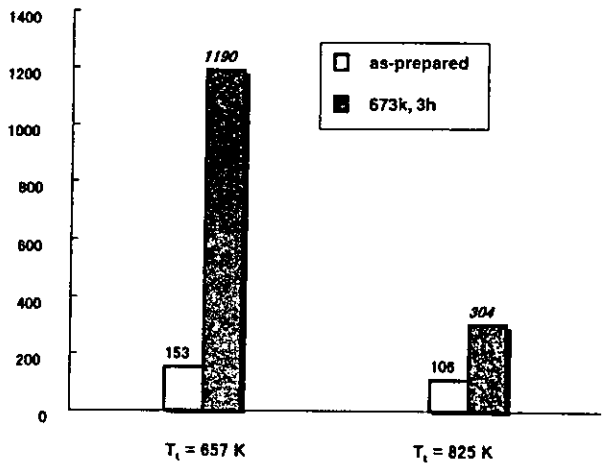

FIG. 3. Enhancement of H_c in FePt particles with different transition temperature (T_t) synthesized under varying Pt ion concentrations in ethylene glycol.

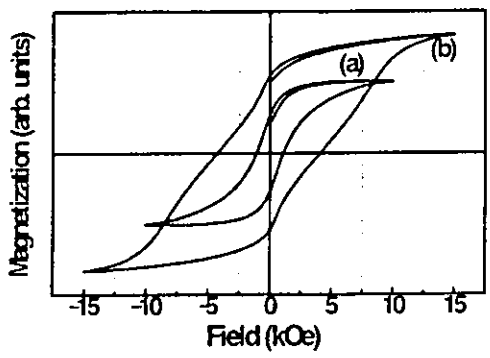

FIG. 4. The hysteresis loops of FePt with T_f of 593 K for (a) as-prepared and (b) annealed at 673 K in H_2/N_2 atmosphere for an hour.

tions and is considered due to atomically ordered islands within the particle that triggers ordering even with less thermal energy. Furthermore, by comparing the results in Figs. 3 and 4, it could be said that the atomically ordered fraction is higher in particles with lower T_f. It is believed that further reduction in reaction kinetic will increase the ordered fraction within the particle assembly and consequently lead to direct synthesis of fct-FePt particles. Experiments aimed at retarding the reaction kinetics through lowering the reaction temperature, type of polyol, etc., are in progress.

IV. CONCLUSION

We conclude that controlling the reaction kinetics results in a reduction of transition temperature. The FePt particles prepared under optimum concentration were 3–4 nm in diameter with T_f of 593 K and H_c of 1.11 kOe at RT. Pt ion concentration in the polyol was found to be one of the parameters that retards the reaction kinetics of the reduction process very effectively. Furthermore, it could be said that regulating parameters such as reaction temperature and type of polyol could pave the way for further reduction in transformation temperature and consequently lead to direct synthesis of fct-FePt.

[1] S. Sun, C. B. Murray, D. Weller, L. Folks, and A. Moser, Science **287**, 1989 (2000).
[2] O. Kitakami, Y. Shimada, K. Oikawa, H. Daimon, and K. Fukamichi, Appl. Phys. Lett. **78**, 1104 (2001).
[3] T. Maeda, T. Kai, A. Kikitsu, T. Nagase, and J. Akiyama, Appl. Phys. Lett. **80**, 2147 (2002).
[4] G. Viau, F. Fievet-Vincent, and F. Fievet, J. Mater. Chem. **6**, 1047 (1996).
[5] O. Perales-Perez, B. Jeyadevan, C. N. Chinnasamy, K. Tohji, and A. Kasuya, *Proceedings of the International Symposium on Cluster Assembled Mater* (IPAP Conf. Series **3**, 2001), p. 105.
[6] B. Jeyadevan, O. P. Perez, C. N. Chinnasamy, K. Shinoda, and K. Tohji, MMIJ Meeting, 133 (2002).

Polyol-process-derived CoPt nanoparticles: Structural and magnetic properties

C. N. Chinnasamy,[a] B. Jeyadevan,[b] K. Shinoda, and K. Tohji
Department of Geoscience and Technology, Tohoku University, Sendai 980-8579, Japan

(Presented on 14 November 2002)

We report the synthesis and magnetic properties of CoPt nanoparticles by using the polyol process. Since the reduction potential of Pt is more positive than Co, Pt is easily reduced compared to Co. Hence, CoPt nanoparticles were realized by coreducing cobalt and platinum acetylacetonate in the presence of an appropriate amount of OH ions in trimethylene glycol. X-ray diffraction and transmission electron microscopy studies showed that the as-synthesized CoPt nanoparticles had fcc structure and about 5 nm in diameter. Composition analysis reveals that the as-synthesized particles are almost equiatomic $Co_{50}Pt_{50}$. Magnetic characterization revealed that these nanoparticles are ferromagnetic at room temperature, and that the magnetization and coercivity values were 8 emu/g and 380 Oe, respectively. Differential scanning calorimetry studies showed that the ordering temperature of the as-synthesized particles was only 550 °C (peak temperature), against 825 °C of the bulk. Annealing the CoPt nanoparticles above 550 °C induced ordering with enhanced magnetic properties. © *2003 American Institute of Physics.* [DOI: 10.1063/1.1558259]

I. INTRODUCTION

CoPt alloy is one of the candidates for high-density storage media due to its high anisotropy (about 4×10^7 erg/cm^3), good chemical stability, and corrosion resistance. According to the phase diagram for bulk Co–Pt alloys,[1] there are two atomic order–disorder transformation regions, namely, the allotropic CoPt and $CoPt_3$. Near equiatomic composition, it exhibits a disorder (A1 phase)–order ($L1_0$ phase) transformation below 825 °C. The $L1_0$ phase with an ordered fct structure is a hard magnetic phase with a high magnetocrystalline anisotropy. Although most of the syntheses to date have focused on thin films, synthesis of nanoparticles by solution chemistry techniques is also gathering momentum to produce Pt-based binary alloy nanoparticles with controlled size and self-assembly.[2] However, the solution chemistry technique cannot directly be applied to synthesize CoPt nanoparticles. For example, the decomposition of $Co_2(CO)_8$ and reduction of $Pt(acac)_2$ under conditions similar to the synthesis of FePt has not yielded CoPt nanoparticles.[2] On the other hand, the use of $Co(CO)_3NO$ instead of $CO_2(CO)_8$ has been proved useful. However, this process did not yield CoPt with high coercivity, even after annealing at 700 °C.[3] Furthermore, in the reverse micelle technique, strong reducing agents were used for synthesis of CoPt particles.[4,5] However, the difficulty in handling metal particles in aqueous media has prompted the search for alternative methods. Hence, we believe that a one-step process to synthesize binary alloy nanoparticles in an organic medium would be ideal. The polyol process is an efficient technique, in which the solvent acts as a reducing and oxidation-preventing agent in addition to the molecular or atomic level control. However, there is no report claiming CoPt synthesis by polyol process alone. Thus, in the present work, we introduce the synthesis protocol for CoPt alloy particles by polyol process and report their magnetic properties.

II. EXPERIMENT

A. Synthesis

Cobalt acetylacetonate (0.01 M)/platinum acetylacetonate (0.01 M) were dissolved either separately or together in trimethylene glycol (TMEG) (200 ml) in a three-neck flask. The appropriate amounts of NaOH were then dissolved in this solution. The solution was placed in an oil bath and heated to 195 °C with constant mechanical stirring and allowed to reflux for a maximum period of 3.5 h at this temperature. Intermediate samples were also collected for composition analysis. After refluxing for 3.5 h, the suspension was allowed to cool to RT. The black precipitated particles were isolated by centrifuging, and were then washed three

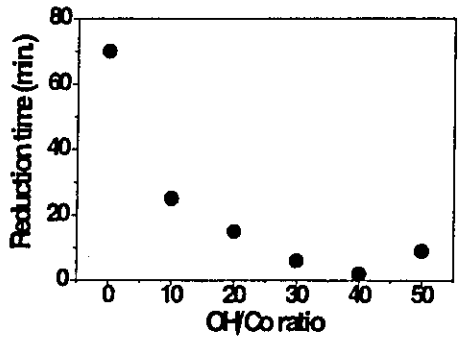

FIG. 1. Effect of OH/Co ratio on the reduction of Co nanoparticles in ethylene glycol.

[a]Electronic mail: chins@cir.tohoku.ac.jp
[b]Electronic mail: jeya@ni4.earth.tohoku.ac.jp

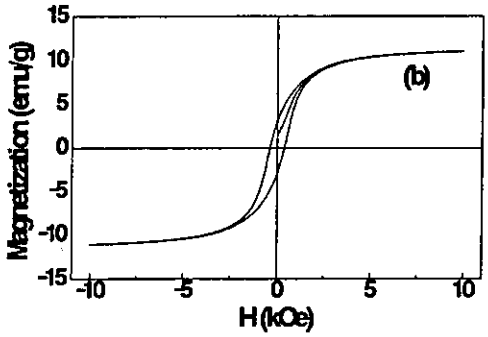

FIG. 2. (a) TEM micrograph and (b) RT hysteresis loop of the as-synthesized CoPt nanoparticles.

times with ethanol to remove the byproducts. As-synthesized samples were annealed in a H_2/N_2 atmosphere for a fixed time of 60 min at different temperatures.

B. Characterization

The crystal structure of the as-synthesized and annealed nanoparticles is studied by using x-ray powder diffraction (XRD) (Rigagu Cu Kα radiation). The morphology was investigated by using transmission electron microscopy (TEM) (acceleration voltage 200 keV, Hitachi HF-2000). The composition analysis was carried out by energy-dispersive x-ray spectroscopy (EDX) attached with TEM. To find the ordering temperature, differential scanning calorimetric (DSC, Rigagu DSC-8270) studies were performed in N_2 atmosphere. Magnetic hysteresis curves were measured using a vibrating sample magnetometer (VSM, Tamakawa model TM-VSM 1230-HHHS) in an applied field of 15 kOe.

III. RESULTS AND DISCUSSION

Since the reduction potentials of Co and Pt are -0.28 and 1.2 V, respectively,[6] Pt is easily reduced compared to Co. Hence, it is important to accelerate the reduction rate of Co to materialize the synthesis of CoPt particles. Authors have found that the reduction rate of Co could be enhanced by introducing an appropriate amount of OH ions in polyol.[7] Figure 1 shows the reduction time versus OH/Co ratio for the synthesis of Co nanoparticles. Without OH ions, cobalt metal precursor in ethylene glycol takes about 70 min to reduce to

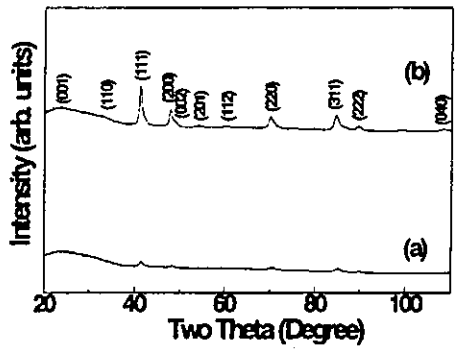

FIG. 3. XRD pattern of CoPt nanoparticles annealed at (a) 500 and (b) 600 °C for 60 min in H_2/N_2 atmosphere.

Co. However, when the OH/Co ratio was 40, the Co ions were reduced to Co in 120 s. This systematic shortening in reaction time could be attributed to the speeding up of the "reaction-rate-controlling step" involved with the metal formation.[6] Here, the dissolution of the intermediate could be considered as the rate-controlling step. Therefore, the excess of hydroxyl ions would have increased the solubility of the intermediate, favoring a very quick generation of dissolved Co species that are finally reduced into metal. Beyond the optimum OH/Co ratio, dissolution of the metal precursors takes place due to the high alkaline condition. XRD analysis showed that the Co metal particles with an average grain size of 15 nm had both hcp and fcc phases, irrespective of OH-ion concentration. The RT magnetization and coercivity values varied between 109 and 144 emu/g and 175 and 214 Oe, respectively. Based on these results, CoPt nanoparticles were prepared by the simultaneous reduction of cobalt acetylacetonate and platinum acetylacetonate in TMEG with appropriate amount of OH ions. Even though the individual Co and Pt reduction time was short with OH ions, we allowed the reaction to continue for 3.5 h. Composition analyses of the intermediate samples demonstrated that the release of Co ions increased with reaction time. TEM-EDX analysis of the 1- and 2-h synthesized samples has the average compositions of $Co_{30}Pt_{70}$ and $Co_{35}Pt_{65}$, respectively. After 3.5 h, the average composition of the nanoparticle was found to be almost equiatomic.

The XRD pattern reveals that the as-synthesized particles have chemically disordered fcc structure, and the average grain size was found to be 4 ($\pm$1) nm. The TEM micrograph of CoPt nanoparticles in Fig. 2(a) showed an average particle size of 4 nm. The electron diffraction pattern also confirmed the formation of fcc CoPt nanoparticles. RT magnetic studies showed that the as-synthesized CoPt nanoparticles have the magnetization of 8 emu/g and coercivity of 380 Oe, as shown in Fig. 2(b). This may be due to the minor fraction of the particles having enough anisotropy to be ferromagnetic at RT. Around the equiatomic composition, annealing at low temperature induces a transition from disordered fcc to ordered fct ($L1_0$ type) structure. In order to determine the ordering temperature, DSC studies have been carried out from 50 to 800 °C. The heating rate was 20 K/min. An exothermic peak was observed between 500 and

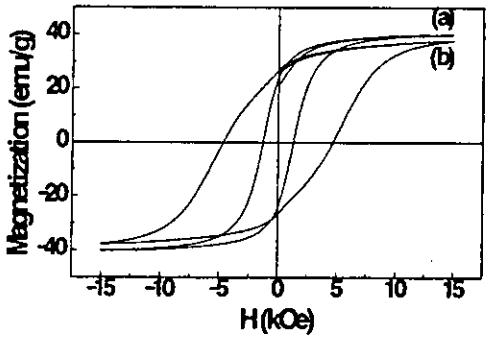

FIG. 4. RT hysteresis loops of CoPt nanoparticles annealed at (a) 500 and (b) 600 °C for 60 min in H_2/N_2 atmosphere.

570 °C (peak temperature: 550 °C) represented that the ordering temperature of the as-prepared CoPt nanoparticles was less than that of the bulk (825 °C). Based on the DSC results, as-synthesized CoPt nanoparticles were annealed at 500 and 600 °C in H_2/N_2 atmosphere for a constant annealing time of 60 min to transform the particles to the ordered fct ($L1_0$) structure. The XRD pattern of the annealed samples is shown in Figs. 3(a) and 3(b). Increase in the intensity of the superlattice peaks with temperature was due to the increase in ordered volume fraction. The RT hysteresis loop of the annealed samples is shown in Fig. 4. The coercivity values are 1.34 and 3.67 kOe for the samples annealed at 500 and 600 °C, respectively. The higher value of coercivity was due to the presence of large number of fct crystals that induced high magnetocrystalline anisotropy. The degree of atomic ordering can be enhanced either by annealing at low temperature for a longer period of time, or vice versa. This was demonstrated as well by an enormous increase in coercivity to 7.57 kOe, when the particles were annealed 700 °C in H_2/N_2 atmosphere for 60 min. These results confirm that nanoparticle CoPt alloys can be synthesized by modified polyol process alone.

IV. CONCLUSIONS

In summary, we have prepared CoPt nanoparticles by using the polyol process alone. The as-synthesized particles were ferromagnetic with magnetization of 8 emu/g and coercivity of 380 Oe. DSC studies showed that the ordering temperature was about 550 °C and that annealing above this temperature induced high degree of atomic ordering and magnetic properties. Studies are in progress to reduce the ordering temperature to make these particles for magnetic recording applications.

ACKNOWLEDGMENT

The Japan Society for the Promotion of Science Program supported this work.

[1] T. B. Massalski, *Binary Alloy Phase Diagrams* (ASM International, Ohio, 1996).
[2] S. Sun, C. B. Murray, D. Weller, L. Folks, and A. Moser, Science **287**, 1989 (2000).
[3] M. Chen and D. E. Nikles, J. Appl. Phys. **91**, 8477 (2002).
[4] E. E. Carpenter, C. T. Seip, and C. J. O'Connor, J. Appl. Phys. **85**, 5184 (1999).
[5] A. Kumbahar, L. Spinu, F. Agnol, K. Y. Wang, W. Zhou, and C. J. O'Connor, IEEE Trans. Magn. **37**, 2216 (2001).
[6] D. R. Lide, *CRC Handbook of Chemistry and Physics*, 76th ed. (CRC Press, Boca Raton, FL, 1995), pp. 8–21.
[7] O. P. Perez, B. Jeyadevan, C. N. Chinnasamy, K. Tohji, and A. Kasuya, *Proceedings of the International Symposium on Cluster Assembled Materials*, 2001, IPAP Series Vol. 3, p. 105.

Mn–Zn ferrite with higher magnetization for temperature sensitive magnetic fluid

B. Jeyadevan,[a] C. N. Chinnasamy, K. Shinoda, and K. Tohji
Department of Geoscience and Technology, Tohoku University, Sendai, 980-8579, Japan

H. Oka
Department of Electrical and Electronic Engineering, Iwate University, Morioka, Japan

(Presented on 15 November 2002)

A growth-assisted coprecipitation process is proposed to achieve highly magnetic Mn–Zn ferrite particles. In this method, first, the particles were synthesized by coprecipitation under optimum condition. Then, further enhancement in particle size was obtained by using the already prepared particles as seed. The average crystallite size of the particles prepared by the proposed method was 12 nm. Furthermore, the magnetization at 1 T applied field was 50 emu/g compared to 37 emu/g of coprecipitated particles. It should be noted that the Curie temperature of the particles remained similar to the coprecipitated particles suggesting that the composition of the Mn–Zn ferrite particles has not been affected by the modified synthesis technique. The gradient of the magnetization-temperature curve was enhanced as a consequence of the rise in magnetization. These particles could be used for the synthesis of temperature sensitive magnetic fluid with higher magnetization and magnetization-temperature gradient. © *2003 American Institute of Physics.*
[DOI: 10.1063/1.1543135]

I. INTRODUCTION

The magnetic fluid (MF) is considered to have applications in the field of heat transfer in solar systems and cooling of mechanical or electric heat sources. The Mn–Zn ferrite nanoparticles that are the most temperature sensitive among the mixed ferrites, is used in the preparation of temperature sensitive magnetic fluid.[1,2] The temperature dependence of magnetization is very sensitive to the chemical composition of the ferrite. This has been studied in detail and the composition that showed the highest magnetization-temperature gradient has been reported to be $(MnO)_{0.41}(ZnO)_{0.18}(Fe_2O_3)_{0.41}$.[1] Thermomechanical analysis of the MF suggests that the nonuniform magnetic field governs the thermoconvective processes and proper control of the same could make the fluid a very effective heat carrier. However, the Mn–Zn ferrite particles dispersed magnetic fluid considered for the above application has a low-magnetic volume force due to comparatively low magnetization of the particles. Thus, to generate a considerable magnetic volume force, the magnetization of the particle has to be enhanced. As the temperature sensitivity is decided by the composition of ferrite, the enhancement of the magnetization can only be realized through increasing the particle size. The Mn–Zn ferrite synthesized by coprecipitation has the tendency to form smaller sized particles with an average diameter of around 9 nm compared to cobalt ferrite and magnetite. Thus, a technique to synthesis particles with larger diameter that could still be dispersed in water or oil was desired. It is well known that the particle size is closely related to the relative interdependence between the nucleation and growth steps, which in turn, can strongly be affected by the solution chemistry and precipitation conditions. In this article, we report the synthesis technique based on heterogeneous nucleation to increase the average particle diameter of Mn–Zn ferrite and thereby increase the magnetic volume force of the temperature sensitive magnetic fluid.

II. EXPERIMENT

A. Materials and method

All reagents were of analytical grade and were used without further purification. In a typical run following the conventional coprecipitation techniquee, 600 ml of a mixed 0.164 M Fe, 0.82 M Mn, and 0.36 M of Zn solution, was continuously added into the reaction vessel containing 1.81 M NaOH dissolved in 1.5 liters of distilled water under continuous mechanical stirring at 500 rpm. The suspension was sampled during the contact period to determine the reaction time required for ferrite formation. The contact time of 1 h was long enough to permit the dehydration and atomic rearrangement involved with the conversion of the intermediate hydroxide phase into the spinel structure. Mn–Zn ferrite nanoparticles prepared by this standard coprecipitation method yields the maximum magnetization (M_s) of 37 emu/g. However, these nanoparticles are good enough for limited applications and a fine control of the nanoparticles diameter in the single domain region should favor the attainment of higher magnetization. Then, to improve further the magnetic properties of single domain Mn–Zn ferrite nanoparticles, the *in situ* growth of the ferrite particles in the presence of Mn–Zn ferrite seeds was carried out.

[a]Electronic mail: jeya@ni4.earth.tohoku.ac.jp

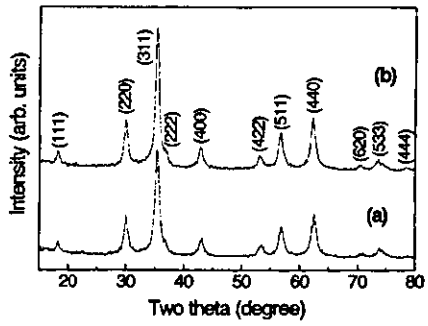

FIG. 1. XRD patterns of Mn–Zn ferrite prepared under (a) the coprecipitation method and (b) the proposed method.

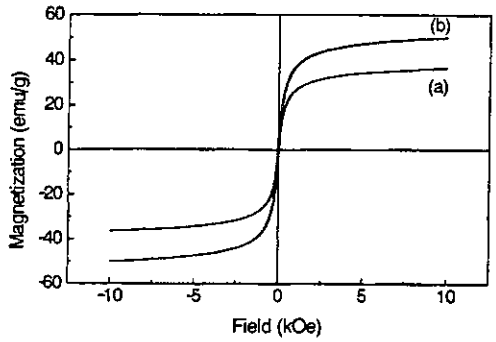

FIG. 2. Hysteresis loops of Mn–Zn ferrite prepared under (a) the coprecipitation method and the (b) proposed method.

B. Characterization

The phases produced during the synthesis of Mn–Zn ferrite particles were analyzed using the x-ray diffraction (XRD) method. The morphology of Mn–Zn ferrite particles was examined by direct observation via high-resolution transmission electron microscopy (Hitachi HF 2000). The specific magnetization (M_s) and coercivity (H_c) of unoriented assemblies of the prepared powders were measured at room temperature in a maximum applied field of 15 kOe using a vibrating sample magnetometer (Tamakawa model TM-VSM1230-HHHS).

III. RESULTS AND DISCUSSION

The heat transfer by conduction in a fluid having a temperature gradient is accompanied by natural convection caused by an inhomogeneous distribution of fluid density. On the other hand, when a magnetic fluid (MF) whose magnetization strongly depends on temperature is heated in a nonuniform magnetic field, the magnitude of the magnetic volume force $\mu_0 M\ \nabla H$, which is also a function of the temperature, will have an inhomogeneous distribution. This induces additional convection termed as "magnetic convection."[3] The magnetization of the Mn–Zn ferrite particles depends on the chemical composition and diameter of the particles.

A. Synthesis of coprecipitated Mn–Zn ferrite

The properties of Mn–Zn ferrite nanoparticles synthesized by coprecipitation depend mostly on parameters such as reaction temperature, and the pH of the suspension. Thus, the particles to be used as seed were synthesized under varying reaction temperature and pH conditions. The variation in magnetization due to the variation in reaction temperature between 80 and 95 °C was very marginal. Similar behavior was observed in the case varying the pH. Thus, the reaction temperature of 95 °C and pH 12.0 was used to synthesis Mn–Zn ferrite with the highest magnetization of 37 emu/g.

TABLE I. Experimental conditions and properties of Mn–Zn ferrite.

Sample code	Conc. of seed, g/l	Metal ion feeding rate, mol/l	Average particle size, nm	M_s, emu/g
S1			9	38
S2	7.7	5×10^{-3}	9	37
S3	7.7	2.5×10^{-3}	12	50
S4	3.75	1.5×10^{-3}	9	40.4
S6	3.75	1×10^{-3}	9	43.4
S7	3.75	0.5×10^{-3}	9	40.1

B. Synthesis of Mn–Zn ferrite by seeding

It is known that the particle size is closely related to the relative interdependence between the nucleation and growth stages, which in turn, can be strongly affected by the solution chemistry and precipitation conditions.[4] As long as the consumption of metal ions for growing Mn–Zn particles is not exceeded by the addition of the same into the solution, no new nuclei form. Since the growth of any one particle is similar to all others, the initial size distribution is largely determined by the time over which the nuclei are formed and begin to grow. The concentration of the metal ions in the suspension at any time during synthesis has to be maintained below the supersaturation concentration to facilitate growth rather than nucleation. An alternative method to achieve separation between the nucleation and growth steps is to use foreign or alike seeds in the reaction media. Thus, in this process, different concentrations of solids is dispersed in

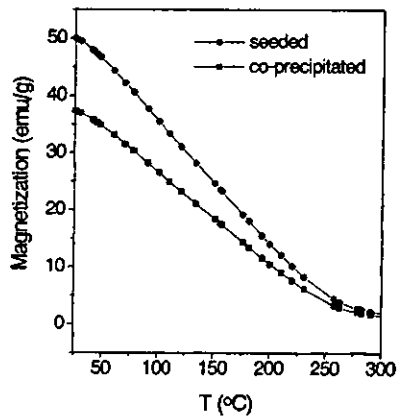

FIG. 3. Thermomagnetization curves of loops of Mn–Zn ferrite prepared under (a) the coprecipitation method and (b) the proposed method.

boiling sodium hydroxide and metal ions are introduced in such a flow rate to keep the concentration below the supersaturation level. Authors have already applied this method for magnetic property enhancement of cobalt ferrite and achieved a coercivity of 4.3 kOe at room temperature.[5] Thus, the flow rate of metal ions introduced to the reaction vessel containing coprecipitated MnZn ferrite in boiling sodium hydroxide as seed, was varied between 5×10^{-3} and 0.5×10^{-3} mol/min, for two levels of seed concentrations. Though a number of experiments were carried out to optimize the condition, the important results are summarized in Table I. The magnetization of the product synthesized under seed concentration of 7.7 g/l and the metal ion feed rate of 2.5×10^{-3} mol/min was the maximum. The magnetization of the ferrite was found sensitive to both seed concentration and metal ion flow rate. The XRD patterns of the coprecipitated and seeded samples are shown in Fig. 1. The average particle size of the seeded sample was 12 nm compared to 9 nm of the coprecipitated. Hysteresis loops of the Mn–Zn ferrite prepared using the conventional coprecipitation method and the proposed method is shown in Fig. 2. The magnetization rose from 37 to 50 emu/g. The enhancement in magnetization has been attributed to the rise in particle size distribution as suggested by the XRD analysis. As a consequence, a rise in magnetization-temperature gradient of the sample could be expected. The thermomagnetization curves of Mn–Zn ferrite samples are shown in Fig. 3. The Curie temperature of the samples did not show any considerable difference suggesting that the modified synthesis process has not affected the composition of the ferrite. However, an enhancement in the magnetization-temperature gradient was observed as anticipated. Thus, organic solvent-based magnetic fluid with higher-temperature sensitivity could be prepared by using the ferrite particles prepared under the optimum condition as dispersant.

IV. CONCLUSION

We have succeeded in synthesizing Mn–Zn ferrite with a larger average diameter by growing the Mn–Zn ferrite seeds used to induce heterogeneous nucleation. As a result, the average particle diameter and magnetization of the particles increased from 9 to 12 nm and 37 to 50 emu/g, respectively. The higher magnetization resulted in a higher magnetization-temperature gradient and could serve as a potential candidate for preparation of temperature sensitive magnetic fluid.

[1] Y. Yamamoto, M. Eng. thesis, Tohoku University, 1988.
[2] N. Yamashita, J. Takahashi, and K. Nakatsuka, Proceedings of the Annual Meeting of Magnetic Fluid Association of Japan, Tokyo (1991).
[3] R. E. Rosensweig, *Ferrohydrodynamics* (Cambridge University, Cambridge, UK, 1985), p. 230.
[4] V. K. La Mer and R. H. Dinegar, J. Am. Chem. Soc. **72**, 4847 (1950).
[5] C. N. Chinnnasamy, B. Jeyadevan, O. P. Perez, K. Tohji, K. Shinoda, and A. Kasuya, IEEE Trans. Magn. **38**, 2640 (2002).